

On the accuracy of simultaneously measuring velocity component statistics in turbulent wall flows with arrays of three or four hot-wire sensors

P. V. Vukoslavčević · J. M. Wallace

Received: 16 April 2011 / Revised: 1 July 2011 / Accepted: 2 July 2011 / Published online: 21 July 2011
© Springer-Verlag 2011

Abstract A highly resolved turbulent channel flow direct numerical simulation (DNS) with $Re_\tau = 200$ has been used to investigate the ability of probes made up of arrays of three or four hot-wire sensors to simultaneously and accurately measure statistics of all three velocity components in turbulent wall flows. Various virtual sensor arrangements have been tested in order to study the effects of position, number of sensors and spatial resolution on the measurements. First, the effective cooling velocity was determined for each sensor of an idealized probe, where the influence of the velocity component tangential to the sensors and flow blockage by the presence of the probe are neglected. Then, simulating the response of the virtual probes to obtain the effective velocities cooling the sensors, velocity component statistics have been calculated neglecting the velocity gradients over the probe sensing area. A strong influence of both mean and fluctuation velocity gradients on measurement accuracy was found. A new three-sensor array configuration designed to minimize the influence of the velocity gradients is proposed, and its accuracy is compared to two-sensor X- and V-array configurations.

1 Introduction

The use of numerical simulations to investigate the characteristics of hot-wire probes and their ability to measure the statistics of turbulent flow fields has provided new insight into sources of measurement error and helped to optimize the probe parameters. Moin and Spalart (1987) studied the spatial resolution effects on the response of an X-array probe with sensor separations of one viscous length as well as the effects of the velocity components in the direction of the sensors' separation. Even with this small sensor separation, they found that the wall normal velocity component root-mean-square (rms) values were significantly overestimated near the wall. Suzuki and Kasagi (1992) extended this analysis by varying the sensor separation of X- and V-array probes using a turbulent channel flow DNS. They found that, although the effects of the out-of-supporting-prongs-plane velocity components are quite small, the rms values of the cross-stream components were greatly overestimated near the wall with increasing sensor separation. Pompeo and Thomann (1993) compared the values of various turbulence statistics from a turbulent channel flow DNS to those from a four-sensor probe with various sensor arrangements. Consistent with previous studies, they also found that the errors became quite large with increasing separation of the sensors.

The influence of sensor separation on the accuracy of the velocity gradient measurements was investigated by Antonia et al. (1993) in a virtual experiment using the direct numerical simulation (DNS) channel flow databases of Kim et al. (1987) and Moser et al. (1989). They also compared the results of this virtual experiment to the values obtained by measurements in a laboratory channel flow with a probe having the same sensor separation as the point separation in the virtual experiment. They

P. V. Vukoslavčević
Department of Mechanical Engineering,
University of Montenegro,
20000 Podgorica, Montenegro
e-mail: petarvuk@ac.me

J. M. Wallace (✉)
Burgers Program for Fluid Dynamics,
University of Maryland, College Park,
MD 20742, USA
e-mail: wallace@umd.edu

showed the strong influence of sensor separation on the measurement accuracy and found that the DNS estimate and experimental results agree well for the sensor separation $\Delta y^+ > 2$. In a recent paper, Vukoslavčević et al. (2009) examined the dependence on the spatial resolution of the important velocity and velocity gradient-based statistical properties measured with a virtual representation of a multi-sensor hot-wire probe using a highly resolved channel flow DNS database. In addition to the idealized sensor response, they also studied the real probe response, the characteristics of which have been determined experimentally. The results of the idealized and real probe response were qualitatively the same, showing that the assumption of the ideal probe response is good enough for a qualitative analysis of the probe resolution parameters.

In the present investigation, the probe's sensors were modeled as points in the simulated flow, so the finite sensor lengths were not accounted for. Moreover, the probe response has been idealized by neglecting the influence of the velocity component tangential to the sensors and flow blockage by the presence of the prongs. Even with these simplifying assumptions, which were also made in all the previous investigations cited except for that of Suzuki and Kasagi (1992), the study of the sensor separation of X- and V-array probes and the array separation and size of three- and four-sensor array probes used to measure both velocity and velocity gradient components has revealed some of the significant sources of measurement error of the velocity statistics and, by extension, velocity gradient-based statistics.

2 The 3-component velocity probes

The most frequently used probe configurations to measure all three components of the velocity vector are shown in Fig. 1. A set of convenient abbreviations to label them is given in Fig. 1: “PL” for plus, “SQ” for square, “OR” for orthogonal and “T” for three out of the four sensors of the “PL” configuration. These configurations previously have been used as single arrays to measure velocity statistics or in multiple array arrangements to measure velocity and velocity gradient-based statistics.

The “PL” configuration was analyzed by Samet and Einav (1987), Dobbeling et al. (1990), Holzapfel et al. (1994), Lemonis and Dracos (1995), and Van Dijk and Nieuwstadt (2004). It also has been used in multi-array probe arrangements to measure vorticity components and other velocity gradient-based properties by Tsinober et al. (1992) and Vukoslavcevic and Wallace (1996). The “SQ” configuration is a modified version of the Kovaszny (1954) probe. In contrast to the Kovaszny probe design, which had only four supporting prongs and was capable of measuring only the streamwise velocity and vorticity components, the “SQ” configuration has separate prongs for each sensor. It has been analyzed by Vukoslavčević and Wallace (1981), Wittmer et al. (1998) and Marasli et al. (1992). The “OR” configuration is used in a well-known commercial probe from DANTEC (model 55P91). It has been employed by Huffman (1980) and Lekakis et al. (1989), as a single array, and as arrays in multi-array probes by Andreopoulos and Honkan (1996) and Honkan and Andreopoulos (1997). The “T” configuration has been

Fig. 1 Various configurations of hot-wire arrays to simultaneously measure all three velocity components. **a** Plus: “PL” configuration, **b** Square: “SQ” configuration, **c** Orthogonal: “OR” configuration, **d** “T” configuration

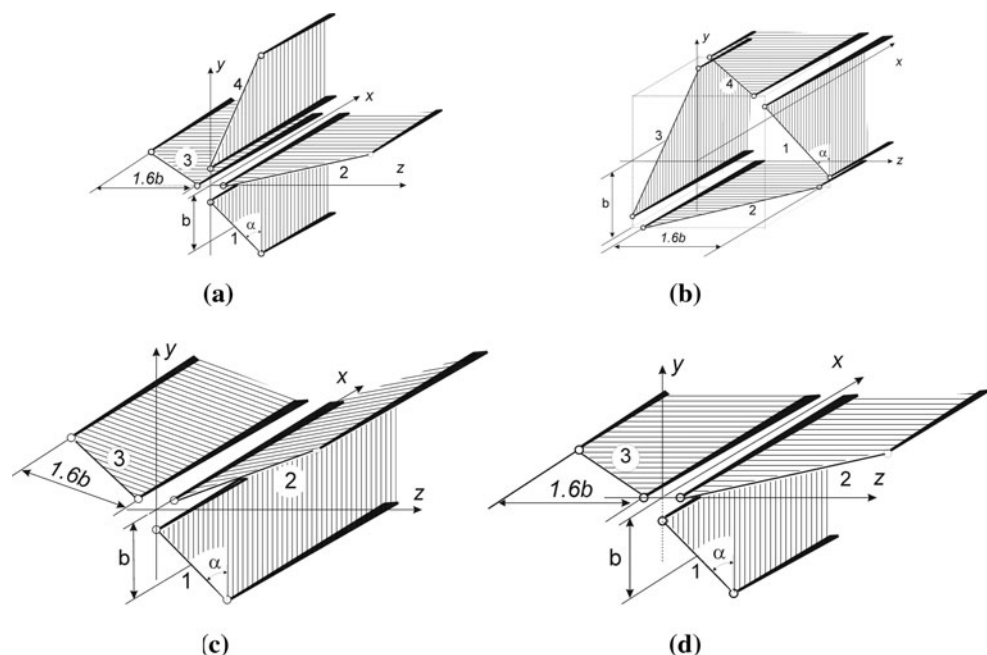
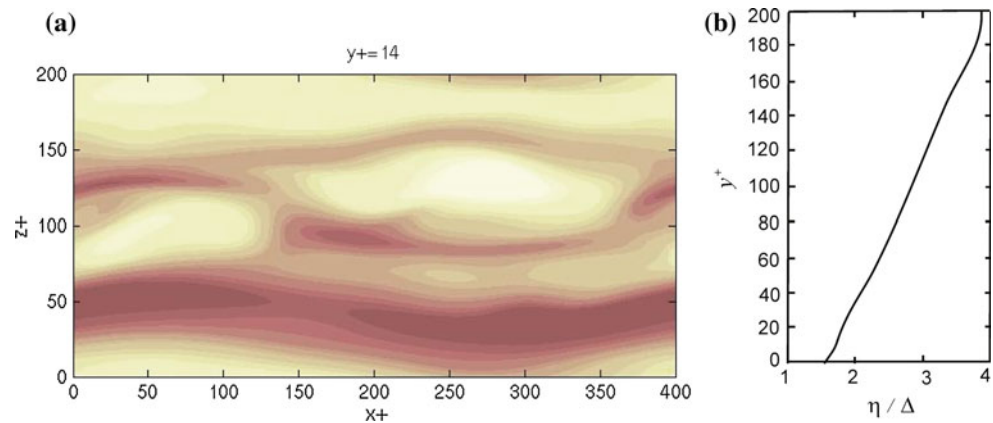


Fig. 2 **a** Contours of the streamwise velocity fluctuations in the minimal turbulent channel flow showing low- and high-speed streaks. **b** Comparison of the grid size, Δ , to the Kolmogorov length, η , across the channel



analyzed by Wallace and Vukoslavčević (1982) as a single array and in arrays of a vorticity probe by Vukoslavčević et al. (1991).

3 Virtual experiment

To simulate the response of hot-wire probes and to investigate their sensor geometrical configurations, the sensors can be thought of as points arranged in the appropriate probe geometry and located on the mesh of a DNS. The relative positions of these points, for a specific configuration and for a given probe spatial resolution defined by the distance b from the array center to the sensor center, is specified in Fig. 1.

To obtain a highly resolved DNS, a minimal turbulent channel flow was simulated for a Reynolds number of $Re_\tau = 200$, where $Re_\tau = u_\tau h/\nu$, u_τ is the friction velocity and h is the channel half-width. The equations of motion were solved using a fractional step method, where both advective and diffusive terms were treated explicitly using an Adams–Bashforth scheme. All spatial derivatives were discretized with second-order, central finite differences on a staggered grid. The details of the numerical methodology can be found in Piomelli et al. (2000), and the first use of this database for this type of study was by Vukoslavčević et al. (2009). The size of the computational domain was set to $2h \times 2h \times h$ and was discretized using $400 \times 400 \times 200$ grid nodes in the streamwise, wall normal and spanwise directions, respectively. The grid was uniform in all directions, and the resulting resolution is $\Delta x^+ = \Delta y^+ = \Delta z^+ \approx 1$, where “+” denotes normalization with the viscous length ν/u_τ . This configuration permits the existence of about two low and high-speed streaks as can be seen in Fig. 2a. The variation of the Kolmogorov length, η , across the channel for this fixed grid spacing is shown in Fig. 2b. Near the wall, the grid size is almost 1.5 times smaller in each coordinate direction than the Kolmogorov length.

To be able to perform the virtual probe experiments, a database of approximately 50 statistically independent instantaneous realizations over 15 eddy turnover times was generated. This sample size was found to be sufficient to obtain converged statistics. The mean velocity and the root-mean-square (rms) velocity and vorticity fluctuation distributions compared very well to those of Kim et al. (1987) at the same Reynolds number.

A virtual probe with the “PL” configuration is shown in Fig. 3. The distance from the array to the sensor centers $b^+ = 2\Delta y = 2\Delta z = 2$. When the sensor centers coincide with the nodes of the grid, the velocity components at each sensor center are equal to the velocity components at the corresponding node. Otherwise, the velocity components at the sensor centers can be found by an adequate interpolation. The same approach has been used for the other configurations shown in Fig. 1, with the same spatial resolution, $b^+ = 2$, which was close to or better than the best spatial resolution of any of the experiments cited in Sect. 2, i.e., about 3η . It follows from Fig. 2b that, for this channel flow DNS, $\eta/\Delta \approx 1.6$ at $y^+ = 15$, which gives $b/\eta = 1.25$. This means that the separation of the sensor centers is about 2.5η and the sensor lengths are about 2η . These values increase closer to the wall and decrease toward the channel centerline.

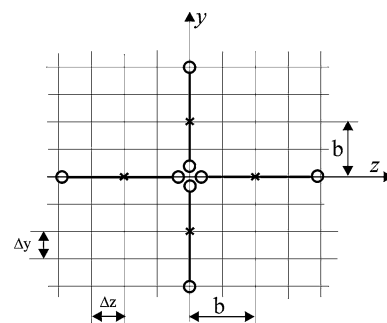


Fig. 3 Sketch of a “PL” configuration shown as points on the DNS grid with $\Delta x^+ = \Delta y^+ = \Delta z^+ \approx 1$ resolution. The distance from the array to the sensor centers is $b^+ = 2$

Using the velocity components at the sensor centers from the DNS, U_i , V_i and W_i , the effective cooling velocity at each sensor center, U_{e_i} , can be found from the expression of Jorgensen (1971),

$$U_e^2 = U_n^2 + k^2 U_t^2 + h^2 U_b^2, \quad (1)$$

where U_n , U_t and U_b are the orthogonal components of the velocity vector with respect to the sensor coordinate system, i.e., normal, tangential and binormal to the sensor, while k and h are the so-called yaw and pitch coefficients that take into account flow distortion by the prongs and thermal effects. Replacing the orthogonal velocity components U_n , U_t and U_b in Jorgensen's expression with U , V and W , the streamwise, cross-stream and spanwise velocity components in the probe coordinate system, the following expressions for the response of the i th ($i = 1-4$ or $i = 1-3$) sensor is obtained:

$$U_{e_i}^2 = a_{i1}U_i^2 + a_{i2}V_i^2 + a_{i3}W_i^2 + a_{i4}U_iV_i + a_{i5}U_iW_i + a_{i6}V_iW_i. \quad (2)$$

The coefficients a_{ij} ($j = 1-6$) depend on the probe geometry, the flow distortion by the prongs and thermal effects. In fact, they are products of sines and cosines of the sensor angle orientations and the pitch and yaw coefficients, h and k , of each sensor. For an ideal probe with specified sensor angle orientations and without prong interference and thermal effects, i.e., $k = 0$ and $h = 1$, they can be defined analytically. For a real probe, an adequate calibration procedure is required to determine the a_{ij} . With these sets of coefficients and effective cooling velocities, the three velocity components at the probe center can be obtained from the set of equations in (2) by neglecting the velocity variation over the probe sensing area, i.e., assuming U_i , V_i , and W_i are the same at each sensor, and applying an adequate numerical algorithm.

By comparing the statistical properties of the simulated flow "measured" in this way by the various configurations of virtual probes with the same properties determined directly from the DNS, the influence of the probe's geometrical arrangements for a given spatial resolution can be systematically examined. In addition, by varying the sensor separations for a given probe geometry, the effects of spatial resolution also can be analyzed.

4 Velocity component statistics

The distribution of the mean streamwise velocity component, \bar{U} , is shown in Fig. 4. The rms distributions of the velocity components, denoted by u' , v' and w' , are shown in Fig. 5, where the values have been normalized by the

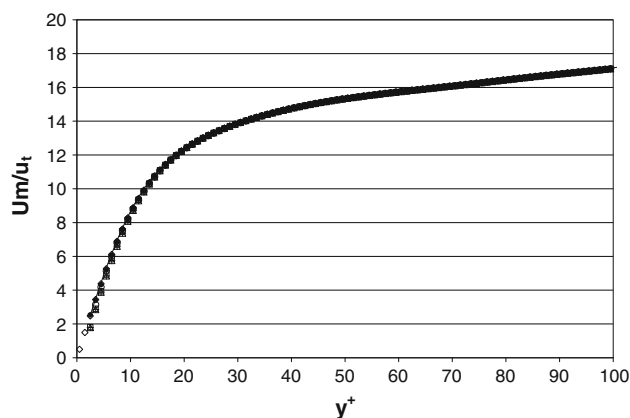


Fig. 4 Comparison of the mean streamwise velocity component profile for various geometrical array configurations and $b^+ = 2$: (empty diamond) DNS, (plus) "PL", (triangle) "T", (square) "SQ", (circle) "OR", (line) X-array

friction velocity, u_τ . The skewness and flatness factors for the velocity fluctuations are shown in Figs. 6 and 7. The distribution values for different array geometrical configurations and the ideal probe case with $b^+ = 2$ are compared to the values of the DNS from which they are determined. They are also compared to the statistics of the u and v velocity fluctuation components obtained with an optimal X-array configuration and to statistics of u and w obtained with an optimal V-array. An optimal V-array consists of sensors 2 and 3 of the "PL" configuration, shown in Fig. 1a, and an optimal X-array of sensors 1 and 3 of the "XL" configuration, shown in Fig. 10a. In order to study the influence of the $\partial\bar{U}/\partial y$ gradient, the statistics obtained with the "SQ" configuration, for which this gradient is assumed known and has been taken into account in the analysis, are also presented.

It is evident that the distribution of \bar{U} and the statistical moments of the u velocity fluctuation component are close to those of the DNS and of each other for all geometrical configurations. They compare very well to the induced values. This means that these statistics are neither affected by velocity gradients nor by the array geometrical configurations, except very slightly with the "OR" configuration. The values obtained with the X- and V-array configurations are the same, so only the X-array data are presented. It is clear that $\partial\bar{U}/\partial y$ can be accurately determined with any of these configurations from the measured mean velocity profile, and its influence can be taken into account in determining the moments of the velocity fluctuations.

In contrast to that of u , the rms distribution of v is strongly affected by the array geometrical configuration, especially close to the wall, in the region of high $\partial\bar{U}/\partial y$ gradient. The most affected are the distributions from the "OR", "PL" and "T" configurations due to their large

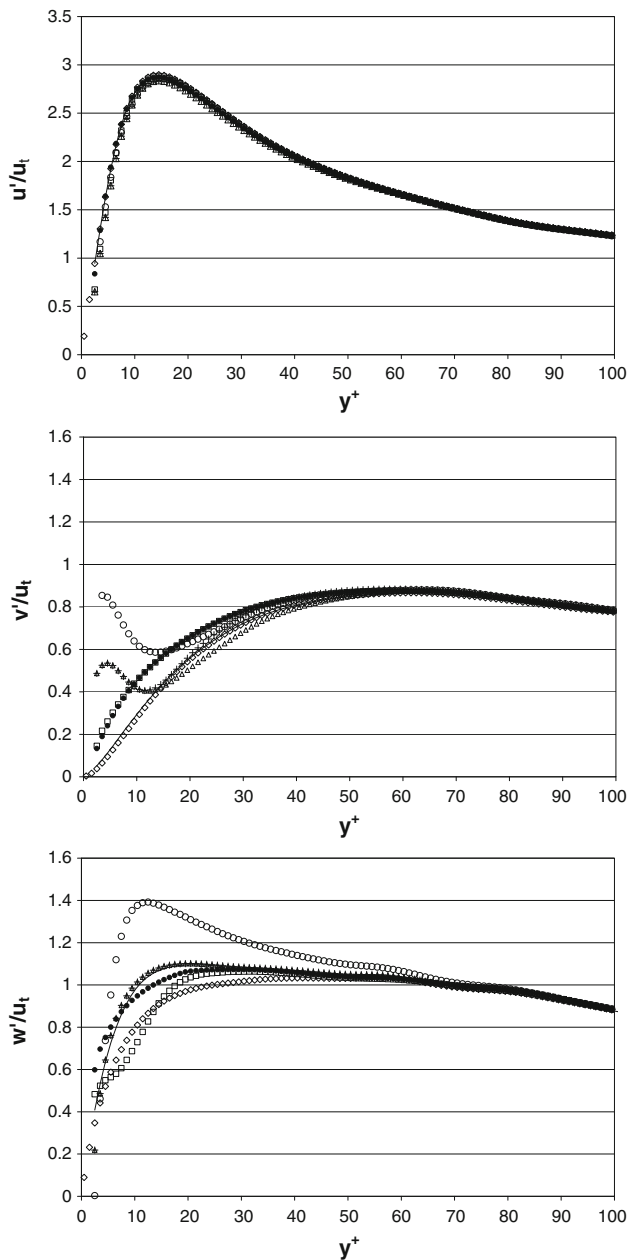


Fig. 5 Comparison of the velocity component fluctuation rms distributions for various geometrical array configurations and $b^+ = 2$: (empty diamond) DNS, (plus) “PL”, (triangle) “T”, (square) “SQ”, (circle) “OR”, (line) X- or V-array, (filled circle) “SQ” with $\partial\bar{U}/\partial y$ included

sensor separations in the y -direction. The rms of v measured by the “SQ” configuration is least affected by the $\partial\bar{U}/\partial y$ gradient, because sensors 1 and 3 (Fig. 1b), that are most sensitive to v , are at the same distance from the wall. These sensors are obviously affected by the instantaneous $\partial U/\partial z$ gradient. The numerical algorithm for the “PL” configuration is constructed so as to choose the optimal three out of the four available sensors. These are usually the upper or lower three sensors. This is why the values

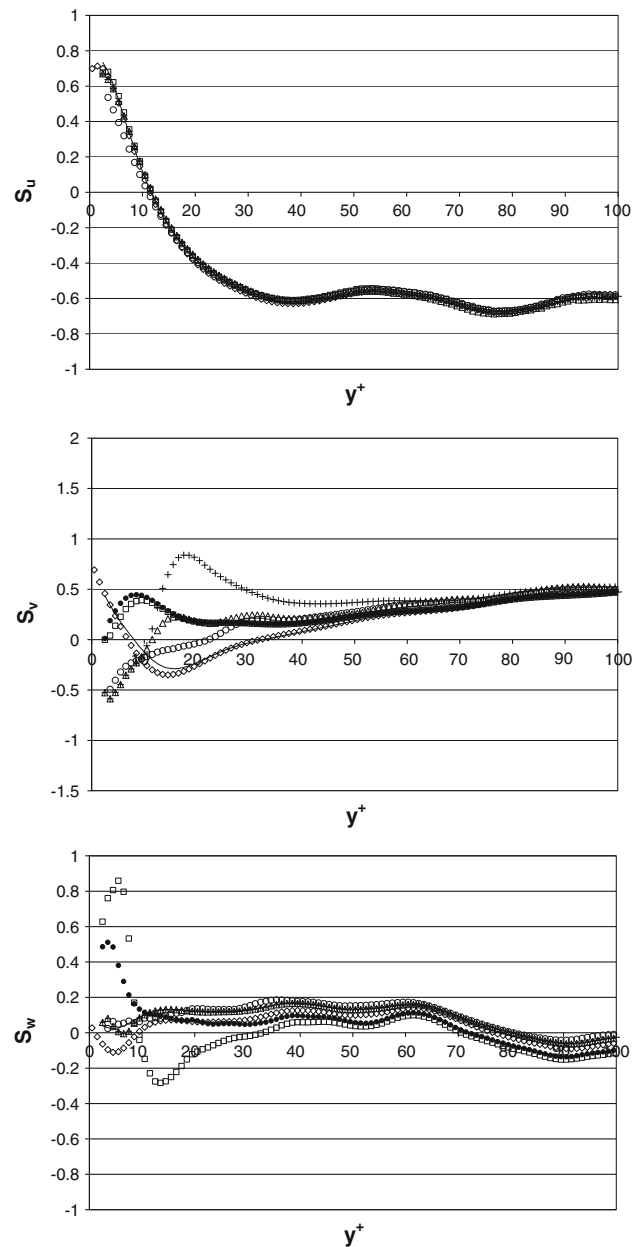


Fig. 6 Comparison of the velocity component fluctuation skewness factor distributions for various geometrical array configurations and $b^+ = 2$: (empty diamond) DNS, (plus) “PL”, (triangle) “T”, (square) “SQ”, (circle) “OR”, (line) X- or V-array, (filled circle) “SQ” with $\partial\bar{U}/\partial y$ included

obtained from the “PL” and “T” configurations are often quite similar. They are also more accurate than the values obtained with the “OR” configuration due to their better spatial resolution in the y -direction.

It is evident from Fig. 6 that the skewness factor, S_w , of the w velocity component is the worse for the “SQ” configuration. This is due to the fact that sensors 2 and 4 (see Fig. 1b) that are mostly sensitive to w , are displaced in the y -direction and are subject to high $\partial U/\partial y$. By contrast, for

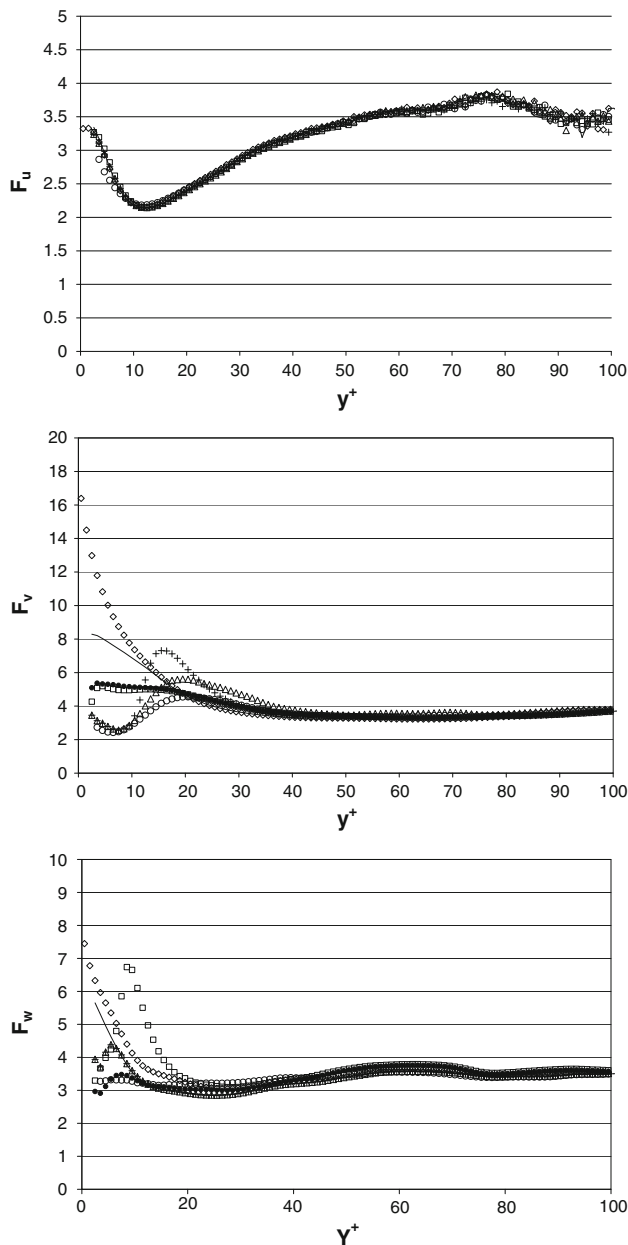


Fig. 7 Comparison of the velocity fluctuation component flatness factor distributions for various geometrical array configurations and $b^+ = 2$: (empty diamond) DNS, (plus) “PL”, (triangle) “T”, (square) “SQ”, (circle) “OR”, (line) X- or V-array, (filled circle) “SQ” with $\partial\bar{U}/\partial y$ included

the “PL” and “T” configurations, the equivalent sensors 2 and 3 are at the same distance from the wall. The rms of the w velocity component is the same for the “PL”-array and the V-array. This means that adding the third sensor in order to account for the binormal cooling velocity component does not make any significant improvement. It is in error due to the strong influence of the velocity gradients in the z -direction. The rms of v obtained by an X-array is even more accurate than the rms of v obtained with the

“SQ”-array. This is because of better spatial resolution in the z -direction of an optimal X-array configuration compared to the “SQ” configuration. This again indicates the strong influence of gradients in the z -direction.

Accounting for the influence of $\partial\bar{U}/\partial y$ did not have any effect on statistics of v measured by the “SQ” configuration. This is to be expected because the sensors that are the most sensitive to v are exposed to the same \bar{U} . By contrast, the statistics of w are strongly affected, especially the skewness factor. Although the result for S_w is improved when $\partial\bar{U}/\partial y$ is accounted for, it is still in large error which is obviously due to the influence of the fluctuation gradient, $\partial u/\partial y$. Surprisingly, the result for the rms of the w fluctuations is somewhat worse than when $\partial\bar{U}/\partial y$ is not taken into account. The influence of accounting for $\partial\bar{U}/\partial y$ was also analyzed for the other configurations. As expected, the statistics of the w velocity component for the “PL” and “T” configurations were not affected while the v component statistics were affected in a similar manner as the w component for the “SQ” configuration.

The variation of the $\bar{u}\bar{v}$ correlation is shown in Fig. 8.

The Reynolds shear stress values are obviously strongly in error for the configurations that also have the v fluctuation velocity statistics in error. These are the “PL”, “T” and “OR” configurations. The “OR” configuration is the worse due to its large sensor separation in the y -direction, while the results for the “PL” and “T” configurations are practically the same close to the wall for the reason explained above when the v fluctuation velocity component statistics were discussed. Besides the X-array, the only configuration that measures the $\bar{u}'\bar{v}'$ correlation for $b^+ = 2$ with reasonable accuracy is the “SQ” configuration.

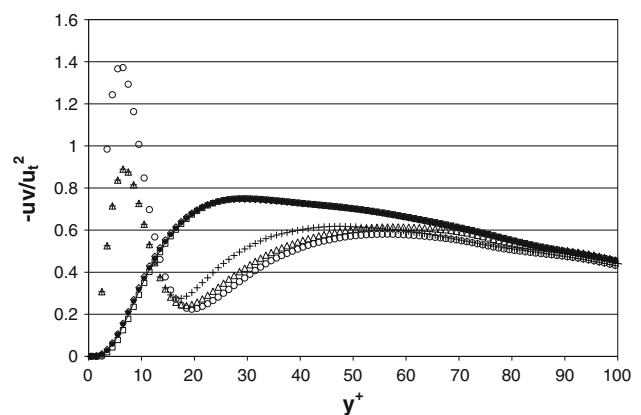


Fig. 8 Comparison of the $\bar{u}\bar{v}$ correlation distribution for various geometrical array configurations and $b^+ = 2$: (empty diamond) DNS, (plus) “PL”, (triangle) “T”, (square) “SQ”, (empty circle) “OR”, (line) X-array, (filled circle) “SQ” with $\partial\bar{U}/\partial y$ included

5 Array configurations to reduce the influence of velocity gradients

There are two possible sources of the large measurement error in most of the velocity statistics presented in Sect. 4. One is that the velocity gradients are neglected over the sensing area of the probes, and the other is the result of falling outside the uniqueness ranges of the probes. The problem of uniqueness range is discussed in detail by Vukoslavčević et al. (2004), among others. The uniqueness range is smallest for the “T” configuration, is larger for the “OR” configuration and is the largest for the “PL” and “SQ” configurations. Due to the fact that the uniqueness range does not depend on the array dimension, it is possible to analyze the influence of the uniqueness range by reducing the probe size close to $b^+ = 0$. In this way the influence of neglecting the velocity gradients is eliminated, and the only possible error is due to the insufficient uniqueness range. We did this analysis and found that, in the case of b^+ almost zero, the induced and measured data are practically identical for all of the statistics and geometrical arrangements shown in Fig. 1. This means that, for this DNS database, the errors are only due to the unavoidable neglecting of the velocity gradients for finite size sensor arrays. In order to reduce these errors, it is obviously necessary to optimize the array geometry so as to reduce the distance from the array to sensor centers in the y - and z -directions. It was expected that, due to the strong $\partial U/\partial y$ gradient present in a turbulent wall layer flow, the separation in the y -direction will affect the accuracy more than the separation in the z -direction.

The first attempt to completely eliminate the influence of the $\partial \bar{U}/\partial y$ gradient was made by Pompeo and Thomann (1993). They proposed the array geometry, shown in Fig. 9, consisting of an X-array in the vertical direction and a V-array in a horizontal plane.

They examined this configuration experimentally and did a numerical analysis, similar to the one presented in this paper, using the numerical database of Hirschberg (1992). They also modeled the sensors as points located in the middle of each sensor with their real response to the flow known from the calibration procedure. They compared the velocity statistics obtained from the virtual

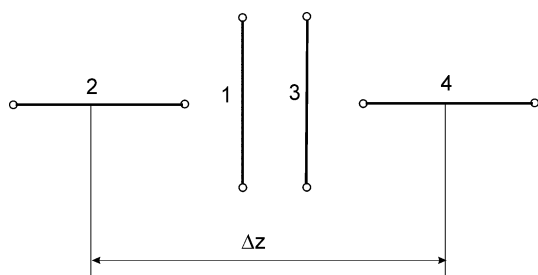


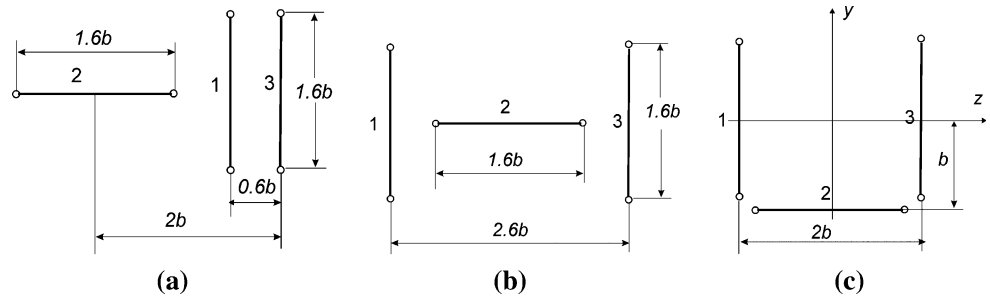
Fig. 9 Front view of the Pompeo and Thomann (1993) probe

experiment to the induced ones at the distance from the wall of $y^+ = 100$ and found that the statistics related to the w velocity component were badly in error. For example, the correlation \overline{wv} for their probe was 50% of the correlation \overline{wv} , although it should be zero from symmetry considerations. It was clear, as they stated, that these large errors are due to the large sensor separation in the z -direction. Making this separation smaller was limited by the prongs separation, number of sensors and prongs, and the interference from the wakes of the sensors. Although the mean velocity gradients in this direction were zero, the errors in the w statistics were obviously due to the instantaneous velocity gradients.

A possibility to reduce the probe size in the z -direction, keeping the same prongs separation and avoiding prongs and sensor wake interference, is to use three instead of four sensors. Three possible configurations are presented in Fig. 10. For the “XL” configuration, sensors 1 and 3, that are mainly sensitive to the U and V velocity components, are close to each other, so these two velocity components should be measured accurately with this arrangement. Sensor 2, which is sensitive to the W velocity component, is positioned to the side of the other two sensors, so this component will be affected by gradients in the z -direction. The overall probe dimension in the z -direction for this arrangement is smaller than in the case of the Pompeo and Thomann probe for the same prongs separations, so the influence of the velocity gradients in the z -direction should be smaller too. For the “H” configuration, the situation is opposite to that of the “XL” configuration. It should measure more accurately the W component rather than the V velocity component. In contrast to the “XL” and “H” configurations, which have zero separations in the y -direction and rather large separations in the z -direction, the “U” configuration is a compromise arrangement obtained by minimizing the separation in both directions.

The uniqueness range of the Pompeo and Thomann probe is the same as for the “PL”- and “SQ”-arrays, because the uniqueness range does not depend on either the sensor position in the y - and z -directions or on the probe size. By removing one of the sensors, as is the case for the configurations shown in Fig. 10, the uniqueness range is reduced to one equivalent to the “T” configuration array. As was discussed at the beginning of this section, the uniqueness range is still large enough for the DNS database used for this analysis. If necessary, for a real probe designed for measurements in a particular turbulent flow, it can be increased by changing the sensor inclination angle while maintaining the same number of sensors, as discussed by Petrović et al. (2010). The distance between the sensor centers, for all configurations shown in Fig. 10, was chosen to avoid the wake interference in the pitch and yaw angle range of $\pm 30^\circ$, which was sufficient for this DNS flow.

Fig. 10 Front view of proposed new configurations of three-sensor probes. **a** “XL” configuration, **b** “H” configuration, **c** “U” configuration



The distribution of the velocity statistics for the array geometrical configurations shown in Fig. 10, with an ideal probe response and with $b^+ = 2$ are compared to the values from the DNS from which they were determined. The “SQ” configuration data as well as X- or V-array data are also presented to demonstrate the difference between the two-, three- and four-sensor array configurations (Figs. 11–13).

As expected, the U and v statistics are very good for the “XL” configuration, in fact as good as for an optimal X-array. The rms and flatness factor distributions of the w component are even better than for an optimal V-array. Due to the asymmetry of the “XL” configuration, the skewness factor distribution of the w fluctuations is worse than for an optimal V-array or for the “H” configuration. On the other hand the rms and skewness of v are rather bad for the “H” configuration due to the strong influence of the instantaneous gradients in the z -direction. The velocity statistics of the “SQ” and “U” configurations are close to each other. By reducing the distance between sensors 1 and 3 for the “U” configuration in comparison to the “H” configuration, the statistics of the v velocity fluctuation component are improved. Unfortunately, the statistics of the w component get much worse due to the strong influence of the gradients in the y -direction on sensor 2. The distribution of Reynolds shear stress, \overline{uv} , compares very well to simulated values for the “XL” configuration. This is expected because the statistics of u and v are very good for this arrangement. Surprisingly, although the statistics of v are not very good for the other configurations, the \overline{uv} correlation is pretty accurate for the other configurations, especially for the “H” configuration, and compare well to the X-array values (Fig. 14).

6 Conclusions

A virtual experiment carried out to examine the response of various sensor arrangements of hot-wire probes used to simultaneously measure all the three velocity components has demonstrated the strong influence of velocity gradients on the measurement accuracy of velocity statistics in the

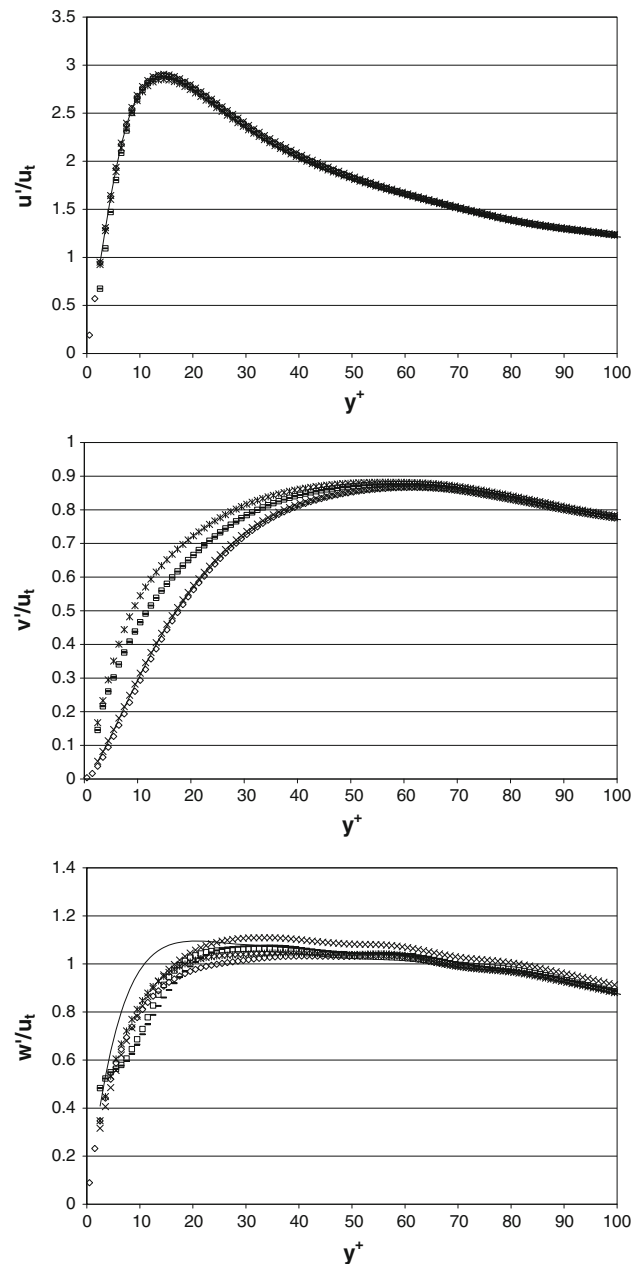


Fig. 11 Comparison of the velocity fluctuation component rms distributions for the new proposed geometrical array configurations in Fig. 10 with $b^+ = 2$: (empty diamond) DNS, (square) “SQ”, (times) “XL”, (asterisk) “H”, (minus) “U”, (line) X- or V-array

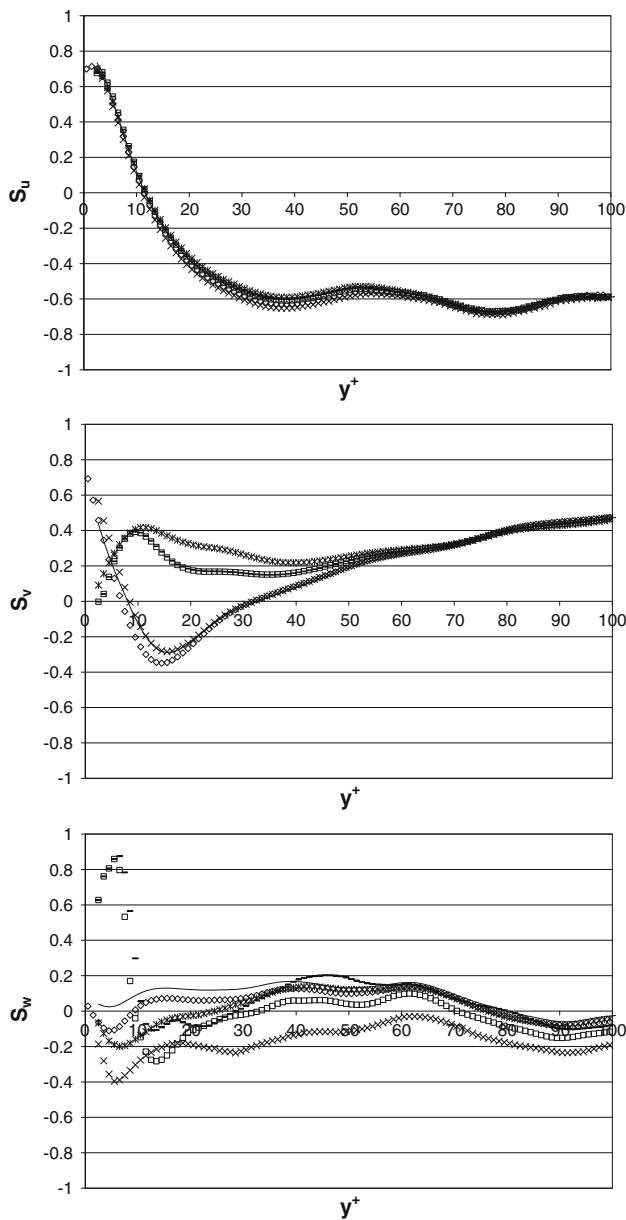


Fig. 12 Comparison of the velocity fluctuation component skewness factor distributions for the new proposed geometrical array configurations in Fig. 10 with $b^+ = 2$: (empty diamond) DNS, (square) “SQ”, (times) “XL”, (asterisk) “H”, (minus) “U”, (line) X- or V-array

near wall region, even for a probe with sensor separations of only several viscous lengths. The investigation was performed assuming an ideal probe response. A much more complex simulation is necessary for a real probe response, but it is expected that the measurements error will be of the same order or larger than in the case of the ideal probe response.

All configurations should accurately measure the velocity statistics as a part of a multi-array probe with a

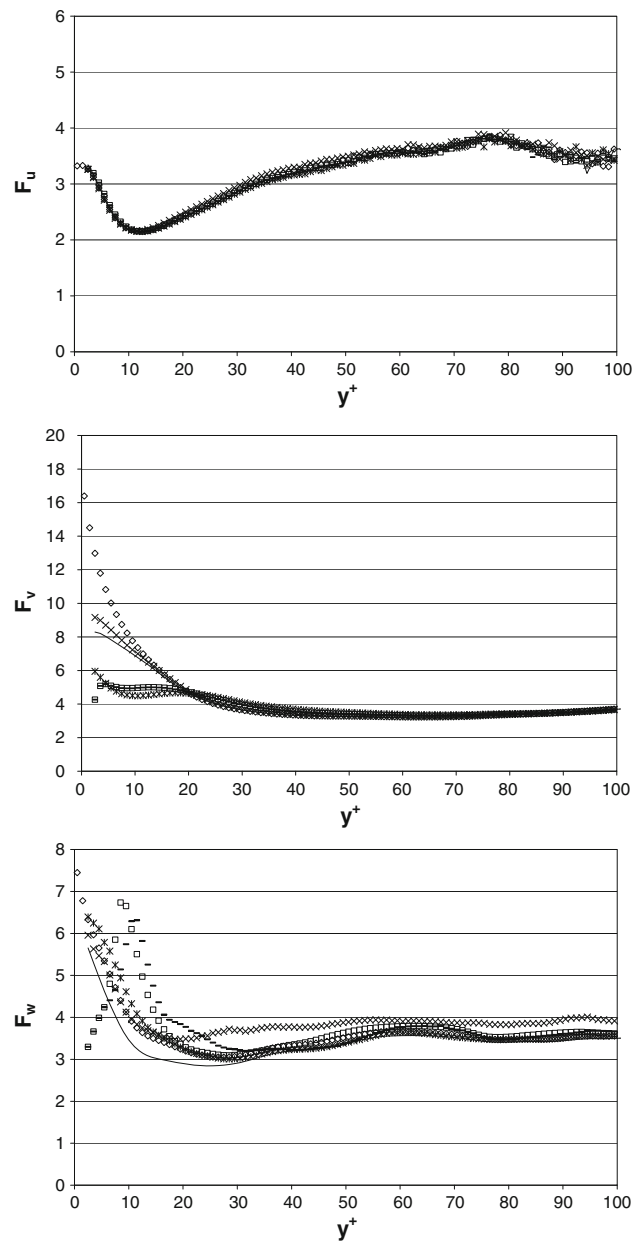


Fig. 13 Comparison of the velocity fluctuation component flatness factor distributions for the new proposed geometrical array configurations in Fig. 10 with $b^+ = 2$: (empty diamond) DNS, (square) “SQ”, (times) “XL”, (asterisk) “H”, (minus) “U”, (line) X- or V-array

spatial resolution sufficient to meet the assumption of linear velocity variation over the probe sensing area. Keeping in mind that it is hard to meet this condition, it is expected that the configuration which performs best, under the assumption of neglecting the velocity gradients, will be least sensitive to the nonlinear velocity variations.

Several general conclusions can be drawn from this study:

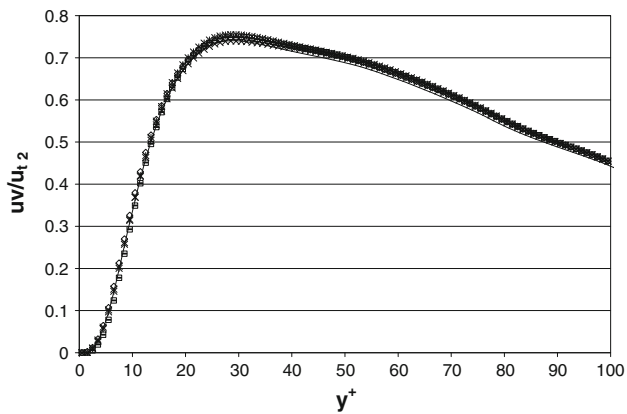


Fig. 14 Comparison of the \overline{uv} correlation distribution for the new proposed geometrical array configurations in Fig. 10 with $b^+ = 2$: (empty diamond) DNS, (square) “SQ”, (times) “XL”, (asterisk) “H”, (minus) “U”, (line) X-array

1. Both, the mean, $\partial \overline{U} / \partial y$ and fluctuating, $\partial u / \partial y$ gradients strongly affect measurement accuracy, so the configurations with minimal dimensions in the y -direction give the best results.
2. Although the mean velocity gradients in the spanwise direction have zero values, depending on the sensors arrangements, the velocity fluctuation gradients in this direction can strongly affect the accuracy of the fluctuation velocity component statistics.
3. Adding a third sensor to account for the binormal cooling velocity component and a fourth sensor in order to increase the uniqueness range does not significantly improve measurement accuracy.
4. The only three-sensor configuration that measures all three components simultaneously with reasonable accuracy comparable to the two-sensor X- and V-arrays is the “XL” configuration.

This study was carried out using a low Reynolds number minimal channel flow database. Thus, the question arises as to its applicability to higher Reynolds numbers. It is fortuitous that, as Reynolds number increases, it has been recently shown [see Smits et al. (2011)] that the relative contribution to the total spectral energy from high wavenumbers decreases because of the increasing influence of larger scale motions. This fact indicates that multi-array probes with sensor configurations and array sizes optimized, as described herein, may be suitable for velocity and velocity gradient measurements at higher Reynolds numbers than are currently accessible via DNS.

Acknowledgments This research was supported by the Ministry of Science and Education of Montenegro. The authors also wish to thank Nicolas Beratlis and Elias Balaras who provided the DNS database used in this investigation.

References

- Andreopoulos Y, Honkan A (1996) Experimental techniques for highly resolved measurements of rotation, strain and dissipation-rate tensors in turbulent flows. *Mes Sci Technol* 7:1462–1476
- Antonia RA, Zhu Y, Kim J (1993) On the measurements of the lateral velocity derivatives in turbulent flows. *Exp Fluids* 15:65–69
- Dobbeling K, Lenze B, Leuckel W (1990) Computer aided calibration and measurements with a quadruple hotwire probe. *Exp Fluids* 8:262–267
- Hirschberg S (1992) Direkte Simulation der turbulenten Taylor-Couette Stromung und der erbenen Kanalstromung. Diss. Pop. ETH, Zurich, Nr.9912
- Holzappel, Lenze B, Leuckel W (1994) Assessment of Quintuple hotwire measurement technique for turbulent flows. *Exp Fluids* 18:100–106
- Honkan A, Andreopoulos Y (1997) Vorticity, strain rate and dissipation characteristics in the near wall region of turbulent boundary layers. *J Fluid Mech* 350:29–96
- Huffman GD (1980) Calibration of triaxial hot-wire probes using a numerical search algorithm. *J Phys E Sci Instrum* 13:1177–1182
- Jorgensen FE (1971) Directional sensitivity of wire and fiber films. *DISA Inform* 13:31–37
- Kim J, Moin P, Moser R (1987) Turbulence statistics in fully developed channel flow at low Reynolds number. *J Fluid Mech* 177:133–166
- Kovaszny LSG (1954) Turbulence measurements. *Physical measurements in gas dynamics and combustion* 10:213. Princeton University Press, Princeton
- Lekakis IC, Adrian RJ, Jones BG (1989) Measurement of velocity vectors with orthogonal and non-orthogonal triple-sensor probes. *Exp Fluids* 7:228–240
- Lemonis G, Dracos T (1995) A new calibration and data reduction method for turbulence measurement by multihotwire probes. *Exp Fluids* 18:319–328
- Marasli B, Nguyen P, Wallace JM (1992) A calibration technique for multiple-sensor hot-wire probes and its application to vorticity measurements in the wake of a circular cylinder. *Exp Fluids* 15:209–218
- Moin P, Spalart PR (1987) Contributions of numerical simulation data bases to the physics, modeling and measurement of turbulence, NASA Tech. Memo 100022
- Moser RD, Kim J, Mansour NN (1989) Direct numerical simulation of turbulent channel flow up to $Re = 590$. *Phys Fluids* 11:943–945
- Petrović DV, Vukoslavčević PV, Wallace JM (2010) Enlarging the uniqueness cone of the nine-sensor, T-configuration probe to measure the velocity vector and the velocity gradient tensor. *Meas Sci Technol* 21:1–8
- Piomelli U, Balaras E, Pascarelli A (2000) Turbulent structures in accelerating boundary layers. *J Turbulence* 1: Art No. N1
- Pompeo L, Thomann H (1993) Quadruple hot-wire probes in a simulated wall flow. *Exp Fluids* 14:145–152
- Samet M, Einav S (1987) A hot-wire technique for simultaneous measurement of instantaneous velocity in 3D flows. *J Phys E Sci Instrum* 20:683–690
- Smits A, McKeon B, Marusic I (2011) High-Reynolds number wall turbulence. *Ann Rev Fluid Mech* 43:353–375
- Suzuki Y, Kasagi N (1992) Evaluation of the hot-wire measurements in wall shear turbulence using a direct numerical simulation database. *Exp Thermal Fluid Sci* 5:69–77
- Tsinober A, Kit E, Dracos T (1992) Experimental investigation of the field of velocity gradients in turbulent flows. *J Fluid Mech* 242:169–192

- Van Dijk A, Nieuwstadt FTM (2004) The calibration of (multi-)hot-wire probes. 2. Velocity calibration. *Exp Fluids* 36:550–564
- Vukoslavčević P, Wallace JM (1981) Influence of velocity gradients on measurements of velocity and streamwise vorticity with hot-wire X-array probes. *Rev Sci Instrm* 52:869–879
- Vukoslavčević P, Wallace JM (1996) A 12-sensor hot-wire probe to measure the velocity and velocity vectors in turbulent flow. *Meas Sci Technol* 7:1451–1461
- Vukoslavčević P, Wallace JM, Balint JL (1991) The velocity and vorticity vector fields of a turbulent boundary layer. Part 1. Simultaneous measurement by hot-wire anemometry. *J Fluid Mech* 228:25–51
- Vukoslavčević PV, Petrović DV, Wallace JM (2004) An analytical approach to the uniqueness problem of hot-wire probes to measure simultaneously three velocity components. *Meas Sci Technol* 15:1848–1854
- Vukoslavčević PV, Beratlis N, Balaras E, Wallace JM, Sun O (2009) On the spatial resolution of velocity and velocity gradient-based turbulence statistics measured with multi-sensor hot-wire probes. *Exp Fluids* 46:109–119
- Wallace JM, Vukoslavčević P (1982) Measurement of the Structure of the Streamwise Vorticity Field in a Turbulent Boundary-Layer. Structure of turbulence in heat and mass transfer 29–42. Hemisphere Publishing Co, New York
- Wittmer KS, Devenport WJ, Zsoldos JS (1998) A four-sensor hot-wire probe system for three-component velocity measurement. *Exp Fluids* 24:416–423